

DEM accuracy evaluation in mountain area by utilizing topographic corrected products of high-resolution TerraSAR-X data

NONAKA, Takashi^{1*} ; OKAJIMA, Yuki¹ ; TSUKAHARA, Koichi¹

¹PASCO CORPORATION

The commercial high-resolution Synthetic Aperture Radar (SAR) sensors have been developed during past few years and became essential source of information in Earth Observation. The production of the maps is examined in the various fields, such as the damaged area caused by disaster, paddy field area, and forest etc. The interpretation of the objects from the images and the positional accuracy of the images are highly important for the map creation and several basic studies for such issues are also conducted by applying high-resolution SAR data.

TerraSAR-X is one of the commercial SAR satellites, and has acquired data worldwide after it was launched in June 2007. Furthermore, TanDEM-X (TerraSAR-X add-on) was launched in 2010. Both satellites are currently acquiring land surface of Earth for creating global and homogeneous Digital Elevation Model (DEM) of very high precision. TerraSAR-X has several processing level products, and the Geocoded Enhanced Ellipsoid Corrected (EEC) is amplitude data projected to the digital elevation model (DEM), which makes possible for users to integrate other optical data and GIS data. Pre-geocoded Single Look Slant Range Complex (SSC) product is complex data with two axes in the azimuth-slant range plane, and used for interferometric and polarimetric analysis.

It was reported that the geometric accuracy of SSC product was better than 1 m in several previous studies, however there are no reports stating details for the validation results of the EEC product using the actual TerraSAR-X data though it is utilized by the most of users. Therefore the authors evaluated the geometric accuracy of the EEC product by performing in-situ experiment using reflectors on the flat area, simultaneously conducted during satellite passed over. The results showed that the accuracy satisfied several meters in case of utilization of SRTM DEM. In the next stage, we developed the model showing the relationships between the geometric accuracy of range direction, DEM accuracy, incidence angle, and it was revealed that the accuracy of the model was about 1 m in the flat area.

The purpose of this study was to evaluate the accuracy of utilized DEM for the topographic correction by applying the model to TerraSAR-X data in the mountain area. The utilized TerraSAR-X data were 2 data sets of high-resolution SpotLight mode (about 2 m resolution) with the different incidence angles, and the DEMs were produced by ASTER with the mesh of 30 m and SRTM with 90 m. We also used the airborne optical data with a geometric accuracy (Digital topographic level of 2,500 scales) for a validation.

Firstly we selected 25 validation points from the intersections and curves of roads easily interpreted both from TerraSAR-X and airborne data. The average, standard deviation, and Root Mean Square Errors (RMSE) value of the difference between TerraSAR-X and reference optical data were evaluated for X-, Y-, and X-Y plane. In the next stage, we examined to apply the model to data in the mountain area. We estimated DEM's errors by assuming that the variation of the differences of the X-direction was corresponded to the errors of the topographic correction since the range direction was almost same for X direction. The results were summarized based on the evaluations of both flat and mountain areas.

Keywords: Geometric accuracy, TerraSAR-X, topographic correction, ASTER, SRTM

Pi-SAR-L2 observation of the landslide caused by Typhoon Wipha on Izu Oshima island

WATANABE, Manabu^{1*} ; DAN, Risako² ; MOTOHKA, Takeshi¹ ; OHKI, Masato¹ ; SHIMADA, Masanobu¹

¹Japan Aerospace Exploration Agency, ²RESTEC

On October 16, 2013, Typhoon Wipha struck Izu Oshima island, and a large-scale landslide was induced by the heavy rain. Six days after the disaster, Pi-SAR-L2 observation was carried out in four different observation directions (L203201?L203204). One Pi-SAR-L observation (L03801) was carried out before the disaster on August 30, 2000 in same observation direction of L203201. The observation data were used to determine which parameters and directions are preferable to detect landslide areas. Several full polarimetric parameters, including Sigma₀, polarimetric coherence, four-component parameters, and eigenvalue decomposition parameters were obtained using PolSARPro and a self-produced programs. As pointed out by Shimada et al. [1], the change of the land cover from a forest before the disaster to bare soil after the disaster was well detected by the coherence between HH and VV. In addition to this parameter, the eigenvalues and four-component decomposition parameters have the potential to detect landslide areas. The data from observations of the bottom to the top of the landslide detect the landslide well, whereas the observation of the opposite side are not as useful.

Soil from the landslide intruded into the town areas, but none of the full polarimetric parameters show any significant difference between the landslide-affected town areas and the unaffected areas.

[1] Masanobu Shimada, Manabu Watanabe, Noriyuki Kawano, Masato Ohki, Takeshi Motooka, and Yutaka Wada, Detecting Mountainous Landslides by SAR polarimetry: A Comparative Study Using Pi-SAR-L2 and X band SARs, Transactions of the Japan Society for Aeronautical and Space Sciences, Aerospace Technology Japan, 2014, 12, No.ists29, pp. Pn9-Pn15.

Keywords: Full polarimetry, SAR, disaster

Shoreline change analysis using JERS-1/SAR and ALOS/PALSAR amplitude images

ASAKA, Tomohito^{1*} ; IWASHITA, Keishi¹ ; KUDOU, Katsuteru¹ ; AOYAMA, Sadayoshi¹ ; SUGIMURA, Toshiro²

¹Nihon University, ²Remote Sensing Technology Center of Japan

Aerial photo analysis and bathymetric survey are commonly conducted to investigate the actual conditions and temporal variation in beach transformation. In recent years, satellite-based optical imagery has been more widely used to evaluate coastal erosion. However, defining shoreline edges using optical imagery is difficult because the sand under seawater near the shoreline can often be seen through clear water. On the other hand, synthetic aperture radar (SAR) imagery can be used to interpret the boundary between a sandy beach and seawater; this is possible because the incident radio waves are not transmitted through water, and SAR images can be compared to trace the shoreline. In this work, we examine the potential of shoreline change analysis by using Japanese Earth Resources Satellite 1 (JERS-1)/SAR and Advanced Land Observing Satellite/Phased Array type L-band Synthetic Aperture Radar (ALOS/PALSAR) amplitude images. We consider Kuji?kurihama beach in Chiba Prefecture as our test site; along this beach, the shoreline is almost perpendicular to the SAR antenna beam orientation for the descending orbit.

We propose a three-step automated shoreline-tracing method to assess the temporal variation of the shoreline in the study area; the HH-polarized JERS-1/SAR amplitude image captured on February 22, 1993, and the HH-polarized ALOS/PALSAR amplitude image captured on May 20, 2010 were used for this purpose. In our method, a shoreline is traced as vector data. In the first step, edge pixels in SAR images are identified by using the Laplacian of a Gaussian filter. In the second step, unwanted edge pixels are masked on the basis of a discriminant analysis in which candidate shoreline edge pixels are estimated by using statistical information within a moving window. The criteria for identifying shoreline edge pixels is decided on the basis of previously gathered data, the backscattering average, and the standard deviation, in the training area (30 by 10 pixels) encompassing the sea, shoreline, and land. In the third step, shoreline vector data are generated from continuous candidate shoreline edge pixels by an automated shoreline-tracing algorithm.

The results were verified in two ways. We first verified the location of the shoreline edge in the SAR amplitude images by overlaying multispectral images acquired on dates close to the acquisition dates of the earlier mentioned JERS-1/SAR data and ALOS/PALSAR data: the JERS-1/Optical Sensor (OPS) color composite image acquired on May 3, 1993, and the ALOS/Advanced Visible and Near Infrared Radiometer type 2 (AVNIR-2) color composite image acquired on January 8, 2011, were used for this analysis. Next, we calculated the statistical information of the backscattering data in the JERS-1/SAR and the ALOS/PALSAR amplitude images for our selected training area. It is noteworthy that the backscattering average and standard deviation in the shoreline training area is a unique than anything training area.

Our proposed method reproduces the temporal variation of the shoreline by using JERS-1/SAR and ALOS/PALSAR amplitude images. However, a part of the shoreline extracted using the JERS-1/SAR amplitude image was inaccurate. The speckle noise in the JERS-1/SAR amplitude image and the low spatial resolution of the raw data may have caused these errors. In our future work, we intend to improve the algorithm for JERS-1/SAR data and accumulate backscattering information of shoreline edge areas using SAR amplitude images.

Keywords: backscattering, beach erosion

Glacier observations by airbourne synthetic aperture radar, PiSAR2, at Tateyama, Japan

FURUYA, Masato^{1*} ; FUKUI, Kotaro² ; SUGIYAMA, Shin³ ; SAWAGAKI, Takanobu⁴

¹Hokkaido University, Graduate School of Science, ²Tateyama Caldera Sabo Museum, ³Institute of Low Temperature Science, ⁴Hokkaido University, Graduate School of Environmental Science

Fukui and Iida (2012) reported that three snowy gorges at Tateyama, Japan, were flowing at a rate of 10-30 cm/month and hence could be identified as glaciers. Fukui and Iida's observations are based on ground-based GPS observations. Because glacier flow velocity data sets are one of the fundamental physical quantities to better understand the dynamics, conventional geodetic techniques have been applied, and the measurement accuracy has significantly improved. However, due to the severe environment and logistic problems, SAR-based velocity mapping has been performed with successful results at large glaciers and ice sheets over the past decades. The velocity mapping technique is so called pixel-offset (or feature) tracking. Thus, applying the same technique to the fore-mentioned newly discovered glaciers, we should also be able to detect the spatial distribution of glacier velocities. However, the presently available satellite-based SAR data set does not have enough spatial resolutions to resolve the velocities. In this regard, the 30-cm resolution of Pi-SAR2 seems promising to perform the pixel-offset tracking. Here we report the first observation images of the Japanese glaciers acquired by Pi-SAR2, and will discuss the preliminary report of velocity mapping.

Keywords: SAR, glacier, Tateyama

Monitoring of Ice sheet marginal zone using multi-frequency SAR data

YAMANOKUCHI, Tsutomu^{1*} ; DOI, Koichiro² ; NAKAMURA, Kazuki³ ; AOKI, Shigeru⁴

¹Remote Sensing Technology Center of Japan, ²National Institute of Polar Research, ³Nihon University, ⁴Institute of Low Temperature Science, Hokkaido University

Environment of Antarctic continent and ice sheet marginal zone is quite important for understanding the mass balance of ice, formation of deep ocean water and other cryospheric phenomena. Previous study showed the usefulness of SAR data to understand what is happen on the boundary area between ice sheet and ice shelf by SAR data analysis, and achieved the mapping of ice sheet surface velocity mapping. In recent, many kinds of satellite equipped SAR sensor plan to launch and these data are available through the scientific Research Announcement (RA) or Announcement of Opportunity (AO).

Based on these facts, this study focuses on the use of multi-frequency SAR data for ice sheet marginal zone monitoring. Especially, we focus on the use of InSAR analysis for grounding line extraction, ice flow velocity mapping by offset tracking, and understanding the image feature difference through the interpretation of X-, C- and L- band SAR data. We use X-band data by TerraSAR-X, C-band data by ENVISAT and ERS-1/2, and L-band data by ALOS/PALSAR data. Then, we will try to describe the applicability and prospectives of ALOS-2 / PALSAR-2 data

TerraSAR-X data were provided by DLRs' AO project (Proposal No. HYD1808), ERS-1/2 and ENVISAT data were provided by ESA Cat-1 AO project, (project CIP.7657) and ALOS/PALSAR data were provided by Research Announcement by JAXA PI project (PI No. P1418002).

Keywords: Ice sheet, multi-frequency, SAR

Evaluation of surface roughness, magnetic permeability and dielectric permittivity using polarimetric SAR data

KOIKE, Katsuaki^{1*} ; MASUDA, Takayuki¹ ; SAEPULOH, Asep² ; URAI, Minoru³ ; OMURA, Makoto⁴ ; DOI, Koichiro⁵

¹Graduate School of Eng., Kyoto Univ., ²Bandung Institute of Technology, ³Geological Survey of Japan, AIST, ⁴Dept. Cultural Studies, Univ. Kochi, ⁵National Institute of Polar Research

Synthetic Aperture Radar (SAR) systems have great advantages of observing the Earth surface regardless of meteorological conditions and detecting crustal deformations by Interferometric processing. Another latest technique, polarimetric SAR has also been widely used through its principle that backscattering intensity differs with polarization mode. However, most applications are limited to image classification. In addition, the evaluation method for surface physical properties has not yet been investigated well. To achieve this evaluation from the viewpoints of geological identification and water-content estimation of soils, this study adopts mdPSAR (**m**agnetic permeability and **d**ielectric permittivity from **P**olarimetric **S**ynthetic **A**perture **R**adar) proposed by Saepuloh *et al.* and tries to evaluate roughness, relative magnetic permeability, and relative dielectric permittivity of the surface materials using the HH, VV, and HV mode SAR data.

As the first step of mdPSAR, the surface roughness is calculated from the backscattering coefficient data at the HV mode and an empirical equation based on an assumption of fractal property of the topography (Campbell and Shepard, 1996). Next, using the Small Perturbation Model (Fung and Chen, 2010) of backscattering coefficient and the Nelder-Mead Simplex method (a method of nonlinear optimization), the relative magnetic permeability and the relative dielectric permittivity are calculated by minimizing the difference between the model and the backscattering coefficient data at the HH and VV modes.

The areas around the Tottori sand dunes were selected as a case study of mdPSAR using two scenes of ALOS PALSAR data acquired on 25 October and 27 April 2009. As the result, the average calculation errors were small as about 1% for both the HH and VV modes and the errors were uniform in general over the scenes. The relative dielectric permittivity values of the Tottori sand dunes were evaluated as 13.4 and 10.6. These values correspond with those of wet sands. It is noted that the value is higher in the scene after raining. Higher values of relative magnetic permeability were evaluated in the sand dunes than the surroundings, which is a reasonable trend because the sands are originated from the weathering of granitic rocks containing magnetite. Consequently, the effectiveness of mdPSAR is demonstrated. However, an improvement is necessary for the surface-roughness estimation of the areas occupied by artificial structures such as buildings. This is because the HH mode intensity becomes strong in them.

Application of mdPSAR to the PARSAR data around Syowa Station, Antarctica is in progress. Its purposes are to clarify distribution of outcrops and snow ice areas, melting state of ices, and development of crevasse topography from the spatio-temporal changes of surface roughness and relative dielectric permittivity.

References

Campbell, B.A., Shepard, M.K. (1996) Lava flow surface roughness and depolarized radar scattering, *J. Geophys. Res.*, v. 101 (E8), 18941-18951.

Fung, A.K., Chen, K.S. (2010) *Microwave Scattering and Emission Models for Users*, Artech House, Norwood, MA.

Saepuloh, A., Urai, M., Koike, K., Sumantyo, J.T.S.: An advanced technique to identify surface materials on an active volcano by deriving magnetic permeability and dielectric permittivity from polarimetric SAR data, *IEEE Geosci. & Remote Sens. Lett.* (under review)

Keywords: ALOS PALSAR, polarization mode, backscattering coefficient, nonlinear optimization, Tottori sand dunes

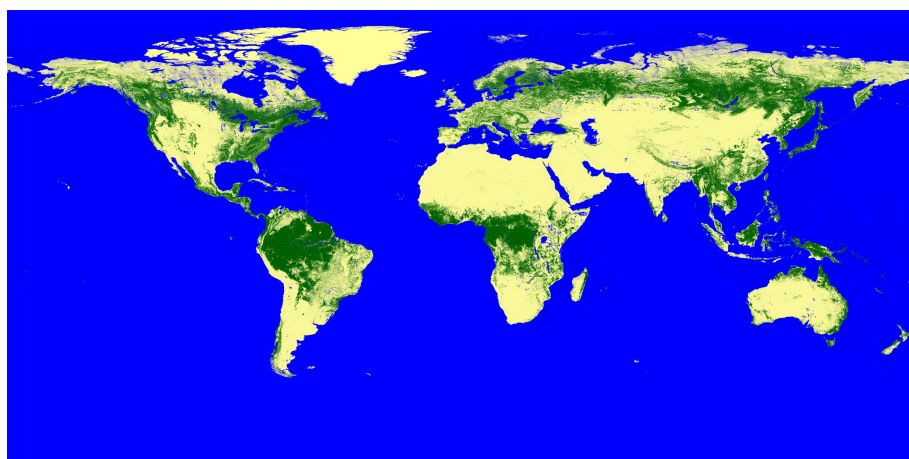
New Global Forest/Non-Forest Maps from ALOS PALSAR data (2007-2010)

SHIMADA, Masanobu^{1*} ; ITOH, Takuya² ; WATANABE, Manabu¹ ; MOTOOKA, Takeshi¹ ; RAJESH, Thapa¹

¹Japan Aerospace Exploration Agency, ²Remote Sensing Technology center of japan

Four global mosaics of Advanced Land Observing Satellite (ALOS) Phased Arrayed L-band Synthetic Aperture Radar (SAR) HH and HV polarization data were generated at 25 m spatial resolution using data acquired annually from 2007 to 2010. Variability in L-band HH and HV gamma-naught for forests was observed between regions, with this attributed to differences in forest structure and vegetation/surface moisture conditions. Region-specific backscatter thresholds were therefore applied to produce from each annual mosaic, a global map of forest and non-forest cover from which maps of forest loss and gain were mapped. Using a combination of Degree Confluence Project (DCP), Forest Resource Assessment (FRA) and Google Earth images as ground data, the overall agreement was 85 %, 91 % and 95 % respectively. Using 2007 as a baseline, decreases of 0.040 and 0.028 dB (with a 0.006 dB confidence level) were observed in the HH and HV gamma-naught respectively suggesting a decrease in forest area and increased smoothing of the global surface at the L-band radar observation. The maps provide a new global resource for documenting the changing extent of forests and contributing to ongoing monitoring through integration with historical (1992-1998) Japanese Earth Resources Satellite (JERS-1) SAR and forthcoming (from 2014) ALOS-2 PALSAR-2 data.

Keywords: SAR, forest/non-forest, SAR mosaic



Recent progress in InSAR and PolSAR signal processing

HIROSE, Akira^{1*}

¹The University of Tokyo

This invited talk reviews latest technology in synthetic aperture radar (SAR) signal processing, in particular interferometric SAR (InSAR) and polarimetric SAR (PolSAR), by focusing on the works on adaptive processing made by the author's group. This field attracts more attention because of its usability in solving serious social problems through, e.g., disaster monitoring and mitigation, water resource management, and prevention of global warming. We discuss a radar-physics-based adaptive processing framework, namely complex-valued neural networks, to increase variety of observation functions and/or improve the accuracy. We also introduce a new phase-unwrapping method to discuss its recent progress.

Keywords: synthetic aperture radar, interferometry, polarimetry, complex-valued neural network, phase unwrapping, Singularity-spreading phase unwrapping

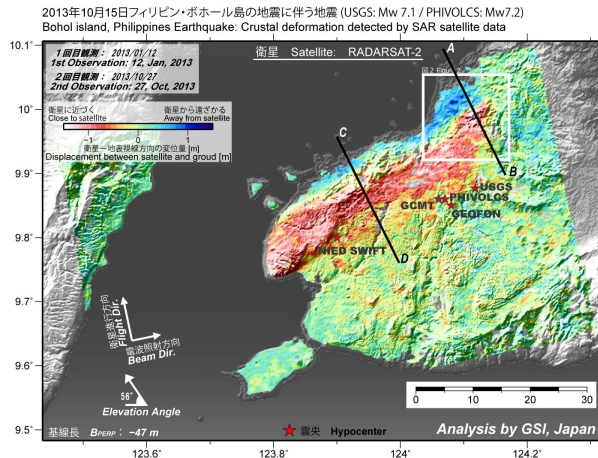
Uplift and reverse fault rupture of the 2013 Bohol earthquake (Mw 7.2), Philippines, revealed by SAR pixel offset analysis

KOBAYASHI, Tomokazu¹ ; TOBITA, Mikio^{1*}

¹GSI of Japan

Applying a pixel offset analysis using RADARSAT-2 SAR data to an inland crustal earthquake that occurred in Bohol Island, Philippines on 15 October, 2013, we succeeded in mapping a ground displacement associated with the earthquake. The most concentrated crustal deformation is located in the northwest of the island with ground displacement exceeding 1 m. The crustal deformation is zonally distributed with the length of approximately 50 km in the ENE-WSW direction. The ground in the mountainous area moves toward the satellite, while in the northern coastal zone the ground moves away from the satellite. A clear displacement discontinuity with the length of about 5 km, probably corresponding to earthquake surface faults, can be identified in the northeastern part. Our fault model that consists of two rectangular planes shows nearly pure reverse fault motions on south-southeast-dipping planes with moderate dip angles. A local rupture located in the northeast occurs at shallow depths, causing appearance of surface ruptures. Applying an additive color process using SAR amplitude images, significant changes in the backscatter intensity are detected along the coast from Maribojoc to Loon, suggesting that the seafloor uplifted and the shoreline shifted seaward resultantly. The area showing the shoreline change is in good spatial agreement with the locally-distributed large ground uplift predicted from our fault model. We can identify a good correlation between the ground upheaval produced by the reverse fault motion and the elevation in the mountainous area, consistent with the idea that the historically-repeated reverse faultings have developed the present-day topography.

Keywords: Bohol earthquake, Crustal Deformation, Pixel offset analysis, uplift, SAR, RADARSAT-2



Estimate of error in ALOS/PALSAR interferograms

HASHIMOTO, Manabu^{1*}

¹DPRI, Kyoto University

Large deformation is generated by the subduction of the Philippine Sea plate in Shikoku. GNSS observation reveals a WNW ward horizontal motion and a velocity gradient from south to north. This velocity field is suitable for the observation with SAR, which is sensible to the E-W ward displacement field. Based on these facts, we have conducted to derive average velocity in Shikoku using ALOS/PALSAR. We mainly analyzed ascending images acquired during 4 years, but anomalously large displacements (peak-to-peak displacement ~ 50 cm) were often observed possibly due to ionospheric disturbances. We discarded interferograms with such disturbances with visual inspection, and stacked rest of them. However we found E-W velocity gradient in Shikoku that is inconsistent with GNSS observations, when stacked interferograms are superposed from 4 paths. Furthermore, discontinuities between paths are evident in the Chugoku district. Therefore we made error estimate in order to clarify its magnitude and spatial distribution, comparing line-of-sight displacements derived from InSAR and GNSS.

The procedure is as follows:

- (1) Calculate displacements of GNSS stations between the acquisitions of master and slave images for a specific pair from the F3 solution of GEONET and convert them to LOS displacements.
- (2) Extract LOS displacements at GNSS sites from the interferogram.
- (3) Take differences of LOS displacements between interferogram and GNSS.
- (4) Examine dependence of latitude, longitude and height, and interpolate differences of LOS displacements with Surface function of GMT.
- (5) Add interpolated differences of LOS displacements to the original interferogram.

One typical example is interferogram for the pair of April 11 and May 27, 2010 for the path 419. Since the time difference is 46 days, little motion is expected. However, we observe LOS changes of ~ 40 cm in the E-W direction. We also find a tongue-shaped region of LOS decrease in the Chugoku district. Applying the above procedure, we obtain interpolated differences of LOS displacement with the opposite sign to the original interferogram. The standard error of difference of LOS displacements for 36 GNSS sites is 7.8 cm. However, the dependences of longitude and latitude are obviously different at 34 N. Therefore we use the Surface function instead of a simple linear function for the interpolation. Finally, we obtain a fairly flat interferogram consistent with the GNSS result. There still remain displacements with shorter wavelength than 20 km, however.

Applying to other pairs, we evaluate standard errors. The minimum is 1.2 cm (Jan. 6 - Feb. 21, 2009), while the maximum is 18.9 cm (May 27 - Jul. 12, 2010). In total 24 pairs, 4 is less than 2 cm, 7 for 2 \sim 4 cm, 6 for 4 \sim 6 cm, 3 for 6 \sim 8 cm, 2 for 8 \sim 10 cm, and 2 is larger than 10 cm. The median is 4.5 cm. For the neighboring path 418 (30 GNSS sites), the minimum is 1.5 cm, while the maximum is 19.8 cm. The median is 4.7 cm. These estimates may give a rough idea of error of PALSAR interferograms including ionospheric disturbances.

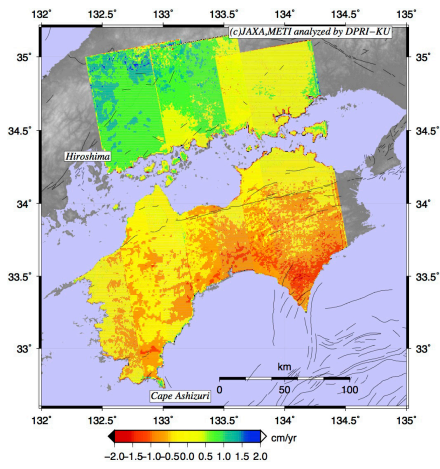
We apply this procedure to other paths (417, 418 and 420) and obtain corrected interferograms that cover the entire Shikoku (Attached figure). This map is fairly consistent with the GNSS velocity field, but there is a discontinuity between the paths 417 and 418. We use interferograms with a rather long perpendicular baseline, which causes decorrelation in mountains. We use only GNSS displacements in plain areas for such interferograms, which results in systematic error.

Keywords: SAR interferometry, PALSAR, ALOS, error, crustal deformation

STT59-10

Room:414

Time:April 29 11:35-11:50



Persistent scatterer SAR interferometry using multi-polarimetric SAR interferograms

ISHITSUKA, Kazuya^{1*} ; TAMURA, Masayuki¹ ; MATSUOKA, Toshifumi¹

¹Graduate School of Engineering, Kyoto University

Persistent scatterer SAR interferometry (PS-InSAR) is a method to estimate surface deformation using a number of SAR interferograms, and has been applied to aseismic fault slip, volcano and land subsidence as a practical monitoring tool. In recent years, more and more satellites that are equipped with SAR, which can acquire multi-polarimetric data has been operated. In this study, we propose a method to processing PS-InSAR analysis using multi-polarimetric SAR interferograms, and show that the estimation accuracy of surface deformation increases.

In this study, we increase estimation accuracy by processing multi-polarimetric SAR interferograms simultaneously. Since, the amount of noise ratio would differ in different multi-polarimetric SAR interferograms depending on the geometry or electromagnetic characteristics of targets, we determine the weighting coefficient between polarimetric SAR interferograms from observed phase based on maximum likelihood method.

We applied the method to ALOS/PALSAR data acquired in multi-polarimetric mode. First, we processed HH-HH and VV-VV interferograms simultaneously. As a result, weighting of HH-HH and VV-VV interferogram was almost identical, suggesting that decorrelation-induced noise in HH-HH and VV-VV interferograms was almost same. In this case, the accuracy of estimated deformation rate would increase twice. On the other hand, when we processed HH-HH and HV-HV interferograms simultaneously, the weighting of HH-HH interferograms are larger than that of HV-HV interferograms, suggesting that HH-HH interferograms has less amount of noise compared with HV-HV interferograms. Nevertheless, we found that the estimation accuracy increases by using both HH-HH and HV-HV interferograms compared with the standard analysis using HH-HH interferograms.

Keywords: persistent scatterer SAR interferometry, surface deformation, polarimetry

Correction by GNSS data for wide area InSAR analysis

MORISHITA, Yu^{1*}

¹GSI of Japan

InSAR results include not only deformation signals but also noises caused by orbital inaccuracies, tropospheric delay and ionospheric delay. Orbital inaccuracies yield a residual orbital phase ramp. As spatial wavelengths of tropospheric and ionospheric noise are typically long, the effect is trivial for a small area but it can be significant for a large area.

Tropospheric noise can be mitigated by estimating the amount of tropospheric delay from a numerical weather model. However, the mitigation does not always work because of the limitation of spatial and temporal resolution of the numerical weather model. There is no common and effective technique to correct ionospheric noise so far while several techniques have been proposed. The ionospheric noise remains a big problem because, in particular, L-band is greatly affected by ionospheric noise. A residual orbital phase ramp can be reduced by flattening the phase in an area with no deformation. Another effective correction method is estimating model parameters (e.g. bilinear surface) to fit other deformation data such as GNSS continuous observation (Tobita et al., 2005; Fukushima and Hooper, 2011). This method works even if the deformation extends the entire area (Kobayashi, 2011). However, if the area is wide, a bilinear surface model is not sufficient because of noises with long wavelengths. A spline interpolation method has been proposed to overcome this problem (Fukushima, 2013).

In this presentation, I will report a GNSS correction technique using a natural interpolation method for scattered points. This technique can mitigate not only residual orbital phase ramps but also noises with long wavelength. Adjusting correction steps enables realistic extrapolations while conventional steps sometimes result in outliers in extrapolated areas. The results of wide area time series InSAR analysis using ALOS/PALSAR data show less noise and more apparent phase changes with shorter wavelength than the interval of the GNSS stations.

References

Tobita, M., H. Munekane, S. Matsuzaka, M. Kato, H. Yarai, M. Murakami, S. Fujiwara, H. Nakagawa and T. Ozawa (2005): Studies on InSAR data processing techniques, Bull. GSI., 106, 37-49 (in Japanese).

Fukushima, Y. and A. Hooper (2011): Crustal deformation after 2004 Niigataken-Chuetsu earthquake, central Japan, investigated by Persistent Scatterer Interferometry, J. Geod. Soc. Japan, 57, 195-214 (in Japanese with English abstract).

Kobayashi, T., M. Tobita, T. Nishimura, A. Suzuki, Y. Noguchi and M. Yamanaka (2011): Crustal deformation map for the 2011 off the Pacific coast of Tohoku Earthquake, detected by InSAR analysis combined with GEONET data, Earth Planets Space, 63, 621-625, 2011.

Fukushima, Y. (2013): Correction of DInSAR noise using GNSS measurements, in proceedings of APSAR 2013, 2013.

Keywords: InSAR, GNSS